Novel GSA-tuned PI Controllers for Grid Integration Scheme of Solar DSTATCOM

Saravanan INDIRANGATHA PANDIAN[1]*, Ponmani CHELLADURAI[2], Vimala VELARUMUGAM[1]

[1] Sankar Polytechnic College, Sankar Nagar, Tirunelveli, Tamil Nadu, 627357, India
sanram1969@gmail.com (**Corresponding author*), v.vimalasivasubramanian@gmail.com

[2] Government College of Engineering, Bodinayakkanur, Tamil Nadu, 625582, India
ponmani@gcetly.ac.in

Abstract: This work presents a novel grid integration scheme for a solar photo voltaic source through a distributed static shunt compensator (DSTATCOM). The proposed system used a Super Lift Luo Converter (SLLC) as an interface between the Solar Photo Voltaic (SPV) source and the DC link of the DSTATCOM. Two Proportional Integral converters were employed for the management of the real and reactive power transactions between the DSTATCOM and the point of common coupling (PCC). Since the grid integration of the harvested SPV energy was carried out by the DSTATCOM and the energy supplied through the SPV channel was unpredictable and varied over a wide range, the tuning of the PI controllers of the DSTATCOM became critical. The novelty of this paper lies in the fact that the two PI controllers of the DSTATCOM were tuned by means of the Gravitational Search Algorithm (GSA). The circuit model of the proposed system was developed in the MATLAB/ SIMULINK environment. Further on, a scaled-down experimental prototype of the proposed model was developed. The obtained simulation results showed that the proposed system which used the GSA for tuning the PI controllers outperformed the Particle Swarm Optimization (PSO) Algorithm and the Ziegler-Nichols based tuning technique.

Keywords: Grid integration of Solar Photo Voltaic power, DSTATCOM, Reactive power compensation, Tuning of PI controllers, Gravitational Search Algorithm.

1. Introduction

The conventional bulk generation of electricity involves huge financial commitments which may be avoided when a large number of government and quasi-government agencies as well as private parties, with multiple funding resources, enter into the field of distributed power generation (Singh & Arya, 2014). Besides, the internationally felt fast depletion of the fossil fuels and the adverse greenhouse effects and the issues related to global warming have led to the consideration of renewable energy sources (Amoozegar, 2016). Renewable energy systems are attractive as it is easier to expand the production capacities flexibly and smoothly over different periods of time (Myneni, Kumar & Sreenivasarao, 2017). The advantages of renewable energy systems have drawn increasing attention and the past few years have witnessed a proliferation of research articles in this area of research (Dheepanchakkravarthy et al., 2018).

A study of the decentralized power generation and its grid integration on the perspective of control system stability has been carried out by Naz et al. (2021). The operation of the DSTATCOM is governed by two controllers which take care of real and reactive power transactions, respectively (Shen & Lewn, 2002). In the absence of any renewable energy source the DSTATCOM is used only for giving the reactive power support (Xu & Li, 2014). This function requires maintaining a prescribed DC link voltage across the DC side capacitor of the DSTATCOM. Proportional and Integral (PI) controllers are predominantly used by many researchers (Eshtehardiha et al., 2007). Different techniques for tuning the PI controllers with the modern tuning algorithms based on heuristic search techniques have been presented by previous researchers. In the place of the two PI controllers required by the DSTATCOM, Fuzzy Logic controllers have been used (Coteli, Besir & Fikret, 2011). Further, the ANN based controllers and the Adaptive Neuro Fuzzy Inference System (ANFIS) based controllers have also been designed, developed and validated by many researchers such as Sherin Jasper (2015) and Badoni, Singh & Singh (2016).

Further, Bhattacharya & Chakraborty (2011) have also demonstrated the applicability of Artificial Neural networks for the management of an active power filter.

Singh & Arya (2014) developed a control algorithm through the power quality improvement for an artificial neural network using a DSTATCOM. Baharudin et al. (2015) have used the Genetic Algorithm (GA) based tuning procedure (Singh & Singh, 2019). Most heuristic algorithms like the PSO, the Grey Wolf Optimization (GWO) Algorithm, the Bacterial Foraging Algorithm (BFA) and the Fruit Fly Optimization Algorithm (FFOA) have been developed based on the behaviour of

https://doi.org/10.24846/v33i3y202407

herds of animals or schools of fish or flocks of birds (Srikakolapu, Arya & Maurya, 2021).

The applicability of several control schemes for the management of the DSTATCOM has been compared in the article of Masand, Jain & Agnihotri (2008). The Gravitational Search Algorithm (GSA) is a completely different one in the sense that the laws of the gravitational force which were the source of inspiration for creating the GSA have been thoroughly studied and validated and had been applied in many engineering applications. The basis from which the GSA has been derived is completely mathematically modelled unlike the other animal behaviour-based search algorithms for which only observational studies have been carried out and which were not fully mathematically modelled (Rashedi et al., 2009). Based on this consideration, in this paper the GSA has been used for the tuning of the two PI controllers of the DSTATCOM. The remainder of this article is as follows. An outline of the proposed system was presented in Section 2.A short review of the Super Lift Luo Converter and the sliding mode controller based MPPT was presented in section 3. In Section 4 the principle of operation of the DSTATCOM and the necessity of employing the two PI controllers for the DSTATCOM are explained. The GSA-based tuning algorithm for the PI controllers is described in Section 5. The simulation of the proposed system and the obtained results are presented in Section 6. The details of the experimental validation and the results obtained therein are specifiedin Section 7. Finally, Section 8 includes the conclusion of this paper.

2. System Outline

As it can be seen in Figure 1, the proposed system consists of a three-phase voltage source derived from the grid which is the main source of power for the load. The load is a linear three-phase load demanding real and reactive power. Between the source and the load, at the Point of Common Coupling (PCC), the DSTATCOM is connected. Between the AC side of the DSTATCOM and the PCC a three-phase passive RL filter unit has been included. A Super Lift Luo Converter (SLLC) acts as the interface between the Solar PV panel and the DSTATCOM.

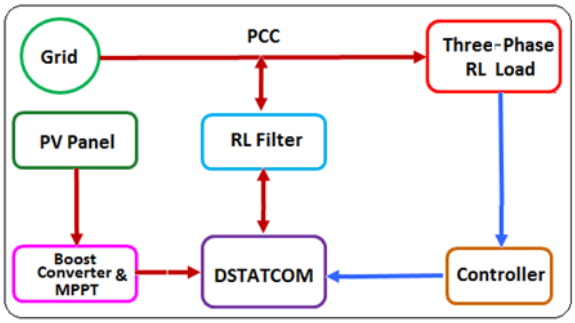

Figure 1. The power flow diagram

Two PI controllers were used in the DSTATCOM for the generation of the reference three-phase signal which is used in the Sinusoidal PWM section that generates the switching pulses for the DSTATCOM. It was noticed that the performance of the GSA-tuned PI controllers is better than that of the PSO-tuned PI controllers. The proposed system was developed in the MATLAB SIMULINK environment and the general system specifications are given in Table 1.

Table 1. System specifications

System / Parameters	Specification
Main Source	3 Ph 50 Hz 380 V
Load	Type 3 Ph 50 Hz 380 V (RL)
Load P (Real Demand)	5000 W
Load Q (Reactive Demand)	5000 VAR
Load PF	0.707 Lag
DSTATCOM	Type 3 Phase Graetz Bridge
DC Link Voltage	1200 V
Filter	R = 15 Ohms ; L = 3 Milli Henry
Solar PV System	4200 W
Interfacing Converter	Super Lift Luo Converter
PV Nominal Voltage	620 V
PV Nominal Current	7

3. Review of the SLLC

As an introductory consideration, Figure 2 shows the topology of the simple lift circuit. The switching pulse generator uses a comparator that compares a triangular carrier and the duty cycle which could vary between 0 and 1. The input voltage of 24 V is stepped up to a high DC output voltage of 169 Volts with a voltage gain of nearly 2.67 obtained for a duty cycle of 0.4.

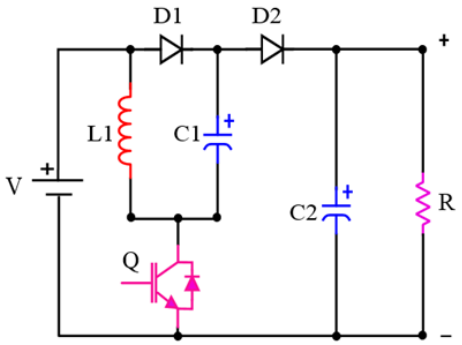

Figure 2. Topology of the Elementary Lift Circuit

While the MOSFET is in the 'ON' state the inductor L1 and the capacitor C1 both come across the input or the source power supply. When the switch is turned off the diode D1 is reverse-biased and the inductor and the capacitor are connected in series and power is delivered to the external load passing through the reverse blocking diode D2. The voltage gain of the simple lift converter is given by equation (1), where V_{in} is the input voltage, V_{out} is the output voltage and D is the duty cycle:

$$voltage \quad gain = \frac{V_{out}}{V_{in}} = \left(\frac{2-D}{1-D}\right) \tag{1}$$

In a multi-stage lift converter, the output of the first stage is the input of the following stage and so on and therefore, in the case of the Re Lift configuration the voltage gain G is given as equation (2):

$$G = \left(\frac{2-D}{1-D}\right)^1 \times \left(\frac{2-D}{1-D}\right)^1 = \left(\frac{2-D}{1-D}\right)^2 \tag{2}$$

A duty cycle of 0.5 gives a voltage gain of 3 for the single lift stage and the voltage gain becomes 9 in the case of the re-lift converter. In a similar manner, the triple lift configuration offers a steady state voltage gain G given as in equation (3). For the same duty cycle of 0.5, a voltage gain of 3 is obtained for the single lift stage but the triple lift configuration as it is shown in Figure 3, produces a voltage gain of 27:

$$G = \left(\frac{2-D}{1-D}\right)^3 \tag{3}$$

In this work the triple lift topology is used for interfacing the Solar Photo Voltaic source with the DC link of the DSTATCOM. Thus if Vin = 10, V and D = 0.8 then the output voltages corresponding to the input voltage for different configurations are as shown in Table 2. Similarly, for Vin = 50 V and D = 0.5, the output voltages corresponding to the input voltage for the three configurations are also shown in Table 2.

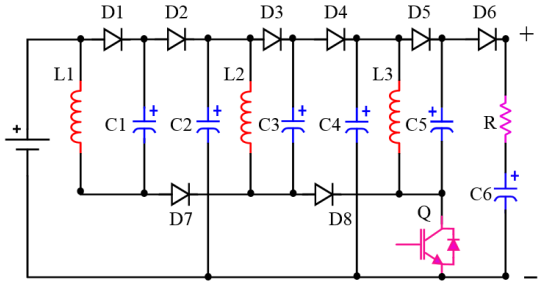

Figure 3. The Triple Lift Luo Converter

Table 2. Comparison of voltage gains of different Lift converters

Configuration	V_{in} (Volts)	Duty Cycle	Voltage Gain	V_{out} (Volts)
Single Lift	10 V	0.8	6	60 V
Re Lift	10 V	0.8	36	360 V
Triple Lift	10 V	0.8	216	2160 V
Single Lift	50 V	0.5	3	150 V
Re Lift	50 V	0.5	9	450 V
Triple Lift	50 V	0.5	27	1350 V

The system uses a sliding mode controller based MPPT. According to the basic principles of the solar photo voltaic source, the maximum power is harvested when the panel is loaded in such a manner that the terminal voltage is equal to the open circuit voltage multiplied by a factor K. The factor K is the ratio between the voltage at P_{max} and the open circuit voltage V_{oc} under standard test conditions. The sliding mode controller allows the switching pulses to the MOSFET of the converter only if the terminal voltage of the SPV source denoted as V_{pv} is higher than the value of $(K * V_{oc})$ If V_{pv} falls below this value, then the switching

pulses are not allowed. A control flag is set when $V_{pv} > K * V$. The control flag is reset when $V_{pv} < K * V_{oc}$. This control flag allows or stops the switching pulses to the gate of the MOSFET of the converter.

4. Structure of DSTATCOM

The three-phase Graetz Bridge structure as shown in Figure 4 is used as the core converter of the DSTATCOM. It consists of a set of three legs each carrying two Power Electronic Switches. The junctions of the upper and lower armsof the three legs form the three-phase terminals. These three-phase terminals are connected to the PCC through a RL filter. The DC link capacitor is connected across the rails of the converter structure.

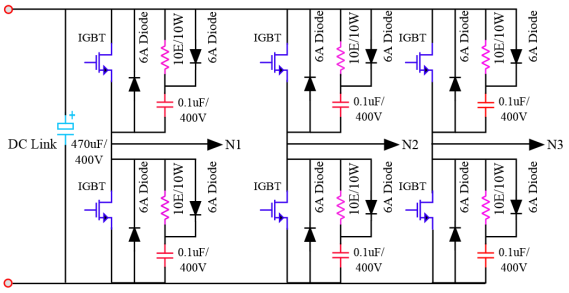

Figure 4. Topology of the DSTATCOM Converter

4.1 Principle of DSTATCOM

Real power P and reactive power Q can be transacted between two power nodes connected through a reactor in accordance with the power transaction equations (4) and (5). Figure 5 (a to d) shows the direction of flow of real and reactive powers depending upon the amplitudes of voltages at PCC and the AC side voltage of the DSTATCOM and the difference in phase angles between these two voltages *V1* and *V2* and connected through a reactor X are defined by equations (4) and (5). With reference to these equations, real power flows from the node where the voltage source leads to towards that node in which the voltage lags. Similarly, the reactive power flows from the higher voltage node to the lower voltage node. With reference to equation (4), if there is no phase difference between the voltages at the two nodes then the real power transaction is zero. However, even if the phase difference between the nodal voltages is zero, there will be reactive power flow from the node with higher voltage to the node with lower voltage as suggested by equation (5).

$$P = \frac{V1 \times V2 \times \sin \partial}{X} \tag{4}$$

$$Q = \frac{V1 \times (V1 - V2) \times \cos \partial}{X} \tag{5}$$

The real and reactive power transactions between Node 1 and Node 2 happen depending upon the differences in the amplitude and phase angle as illustrated in Figures 5(a) to 5(d). Also, from equations (4) and (5) it can be concluded that the amplitude of the reference signal and its phase angle may be manipulated by two different controllers independently for controlling the flow of real and reactive powers.

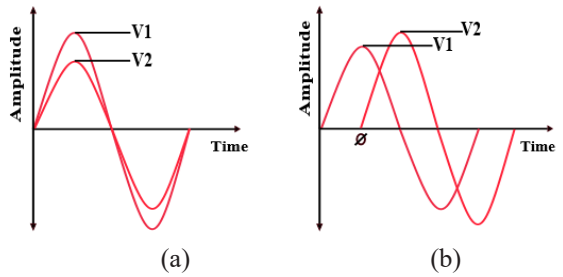

(a) (b)

(a) P = 0; Q: Node 1 to Node 2, (b) P: Node 1 to Node 2; Q: Node 2 to Node 1

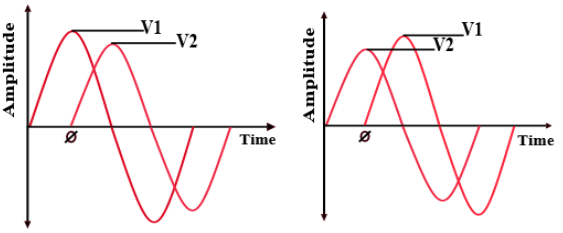

(c) (d)

(c) P: Node 1 to Node 2; Q: Node 1 to Node 2,
(d) P: Node 2 to Node 1; Q: Node 1 to Node 2

Figure 5. Directions of real and reactive power flow

The flow of real power from the PCC to the DC link charges the DC link capacitor and causes the rise of the DC link voltage. Similarly, the flow of real power from the DC link to the PCC discharges the DC link capacitor and causes a fall in the DC link voltage. Thus, the controller that is meant to regulate the DC link voltage controls the magnitude and direction of the flow of real power. The controller meant for regulating the d component of the Park transformed AC three-phase voltages at PCC, controls the magnitude and direction of the flow of reactive power.

The proposed system therefore uses two PI controllers associated with the DSTATCOM. The optimal tuning of the two PI controllers using the GSA is the main focus of this paper.

5. Tuning of PI Controllers

A DSTATCOM commonly uses two PI controllers. A PI or a PID controller is an effective regulatory controller. The performance of the PI controller depends upon the proportional constant Kp and integral constant Ki. The methodology for finding the appropriate values of Kp and Ki is known as tuning the PI controller. When the system is non-linear it becomes difficult to estimate the appropriate values for Kp and Ki.

The Genetic Algorithm, the Particle Swarm Optimization Algorithm and the Grey Wolf Optimization Algorithm are some of the common PI controller tuning algorithms. In this work the Gravitational search algorithm is used. GSA is inspired from the established laws of the Gravitational Forces between different masses considered in a space. The root model has been intensively studied and amenable for easy mathematical modelling.

The Gravitational Search Algorithm (GSA) was proposed by Rashedi et al. (2009). The GSA is a population-based heuristic search algorithm that was inspired by Newton's law of gravity and gravitational interaction forces between the masses considered in a space. The different mass elements used for the population in GSA are called agents. The agents attract each other by virtue of the gravitational forces of attraction between them. The fitness of each agent is estimated by the absolute values of the agents` resultant accrued masses considered at the end of each iteration. During the evolutionary process the agents or particles move towards other heavier particles by the action of the gravitational force of attraction.

At each step, known as the exploration step, a movement of the agents with a wide scope is exhibited. During this phase, the heavier agents or objects move relatively slower. The slow movement of the heavier masses is considered as the exploitation action. As a result, finally the best candidate solution is that object which accrues the heaviest mass when compared with other objects in the population. To start with, let G be the gravitational constant and the value of G at iteration number *t* is given as equation (6):

$$G(t) = G(0)\, e^{\frac{-\alpha t}{T}} \tag{6}$$

The values of function G(0) and of the variable α are initialized at the start of the search process and their magnitudes respectively get reduced during the heuristic search process. *T* is the total number of iterations used until arriving at the final result.

The law of gravitational force as applied to a set of two masses is given by equation (7):

$$F1 = F2 = G\frac{M1 \times M2}{r^2} \tag{7}$$

By Newton's Second law of motion if a force *F* is exerted on an object with a mass M the object accelerates proportionally to the magnitude of the applied force. According to this law the acceleration, the force F and the mass M are related by equation (8):

$$a = \frac{F}{M} \tag{8}$$

There are three kinds of masses associated with each object involved in the process, namely the Active Gravitational mass M_a, the Passive Gravitational mass M_p and the inertial mass M_i The total resultant mass is therefore given as equation (9):

$$F_{ij} = G\,\frac{M_{aj} \times M_{pi}}{R^2} \tag{9}$$

where *Maj* is the Active gravitational mass of object j on object i and *Mpi* is the Passive gravitational mass of object i. If M_i is the inertial mass of object i, the acceleration of the object can be expressed by equation (10):

$$ai = \frac{F_{ij}}{M_{ij}} \tag{10}$$

For each iteration the position and acceleration of each object are modified as given in equations (11) and (12):

$$V_i\,(t+1) = rand\,(i) \times V_i(t) + ai(t) \tag{11}$$

$$X_i\,(t+1) = rand\,(i) \times V_i(t) + ai(t) \tag{12}$$

The important steps in the implementation of the GSA are as follows:

1. Initialize gravitational constant *G0, α,* and the iteration counter *t*;

2. The initial population is generated randomly and there could be *N* objects. The initial inter-object positional relationship or the

initial position of each object with respect to the other objects is given as equation (13):

$$X_i(t) = (x_i^1(t), x_i^2(t) \ldots x_i^d(t) \ldots \ldots x_i^n(t)) \quad (13)$$

where i = 1, 2……. n;

3. The process is repeated until the stopping criteria are reached;

3.1. The strengths of all agents or objects are evaluated. The best and the worst performing objects are identified;

3.2. The current gravitational constant is estimated and updated;

3.3. When object *j* acts on object *i* with force Fij, at a specific time instant (t) the force can be calculated as in equation (14):

$$F_{ij}^d(t) = G(t) \frac{M_{pi}(t) \times M_{aj}(t)}{R_{ij}(t) + \varepsilon} \left(x_j^d(t) - x_i^d(t) \right) \quad (14)$$

where *Maj* is the active gravitational mass of object *j*, ***Mpi*** is the passive gravitational mass of object *i,* and *G(t)* is gravitational constant at time *t*;

3.4. At iteration *t*, calculate the total force acting on object *i* as follows:

$$F_i^d(t) = \sum_{j \in Kbest, j \neq i} rand \; F_{ij}^d(t) \quad (15)$$

where ***Kbest*** is the set of first *K* agents with the best fitness values and biggest masses;

3.5. Calculate the inertial mass as follows:

$$m_i(t) = \frac{f_i t_i - worst(t)}{best(t) - worst(t)}, \quad (16)$$

$$M_i(t) = \frac{m_i(t)}{\sum_{j=1}^{N} m_j(t)}; \quad (17)$$

3.6. The acceleration of the object *i* is calculated as shown in equation (18):

$$a_i(t) = \frac{F_i(t)}{M_{ij}(t)} \quad (18)$$

3.7. The velocity and the position of the object***i*** are found as shown in equations (6) and (7);

3.8. The iteration number gets incremented until the stopping criteria are satisfied;

4. The optimal solution is obtained.

In the proposed GSA-based tuning of the PI controller in the MATLAB SIMULINK environment the Integral Square Error (ISE) is the objective to be minimized. To this effect, the Kp and Ki values used in the PI controller block are to be optimized. The methodology adopted forthis system directly reads the ISE from the MATLAB SIMULINK model and the modifications carried out by the GSA, which are the updates for Kp and Ki are directly entered into the PI controller block. Two m files are used. The first one holds the GSA algorithm. The second m file reads the ISE from the SIMULINK model, interacts with the m file that runs the GSA and then itgets the values for Kp and Ki from the GSA program file and writes the Kp and Ki values straight into the PI controller block inMATLAB SIMULINK. This methodology is more effective than the coinage of a mathematically approximate objective function because the ISE as the objective function, which is obtained from the SIMULINK itself is more effective as it is the result of the complete functional model.

6. Implementation in MATLAB SIMULINK

The circuit model of the proposed system was developed in the MATLAB/SIMULINK environment. Figure 6 shows the solar PV subsystem and the SMC subsystem. The SMC based subsystem produces the switching pulses as per the algorithm implemented in SIMULINK and the switching pulses generated are routed to the power electronic switch of the SLL Converter.

Figure 7 shows the position of the three-phase DSTATCOM, the solar PV subsystem, the controller subsystem and the passive filter sections between the AC side of the DSTATCOM and the PCC.

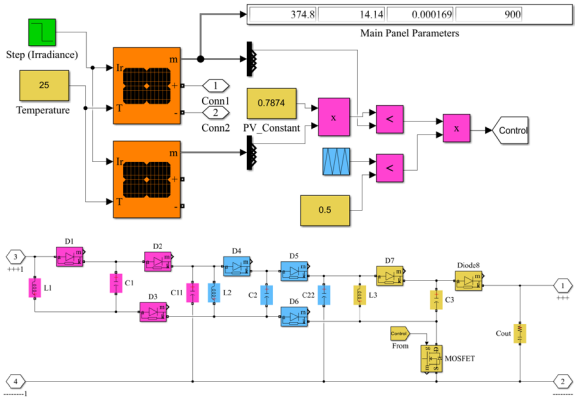

Figure 6. SPV and SLLC Sub-Systems

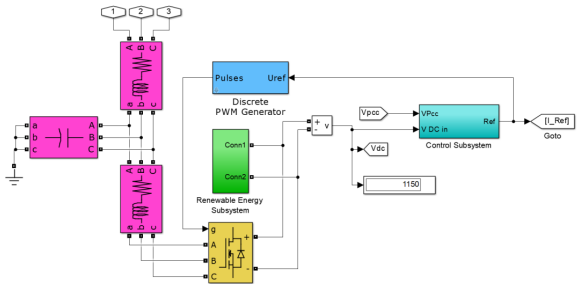

Figure 7. The position of the Three-Phase DSTATCOM

The terminal voltage of the solar PV module is stepped up in three cascaded stages by the SLLC and the resulting output voltages at each stage of the SLLC It can be noted that the change in the solar irradiance causes a step rise in voltage at the output of the first two stages of the SLLC. However, since the output of the third stage is the DC link voltage of the DSTATCOM it is regulated at the 1200 V level for all solar irradiances. However, the power delivered to the DSTATCOM is in the form of a variation in current against a fixed voltage and the solar PV current that changes from 2.3 A to 15.2 A at time = 3 seconds because of the change in the solar irradiance. The change in the solar irradiance causes the power being integrated to rise from 2760 Watts to 18240 Watts. However, if the DC link voltage is maintained at the 1200 V level renewable energy integrated into the DC link of the DSTATCOM is manifested as a variable current wave form in accordance with the variations in the solar PV source.

The performance of the DSTATCOM with respect to the control system performance indices, namely overshoot, settling time number of oscillations, the Integral Square Error (ISE), Rise Time and Steady State Error, was compared with that of the PSO-based tuning technique and the proposed GSA-based tuning technique for PI controllers. Figure 8 shows the voltage at the point of common coupling and the grid DSTATCOM current for the period before the rise of the solar irradiance occurring at 3 seconds. During this period the DSTATCOM receives real power from the grid to handle power losses. Figure 9 shows the voltage at the PCC and the DSTATCOM Grid Current after the solar irradiance has reached 900 W/m^2. The grid voltage and the current supplied by the grid are in phase as shown in Figure 9. The grid injection current from DSTATCOM has reached the value of 15.5 Amperes. The voltage at the PCC and load current are shown in Figure 10. Although the load current is lagging from the voltage at PCC, the source current or the grid current was almost in phase with the voltage at PCC as shown in Figure 9 and the grid side power factor was as high as 0.97, while the load power factor was 0.707 (per phase P = 5 KW; Q = 5 KVAR). The values of Kp and Ki obtained using the Ziegler-Nichols Tuning Algorithm, the PSO algorithm and the GSA algorithm were included in Table 3.

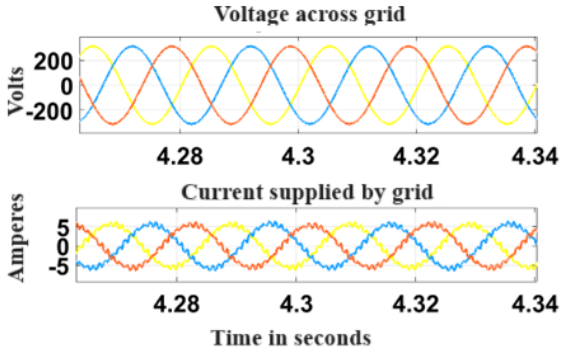

Figure 8. The Voltage at PCC and the current supplied by grid

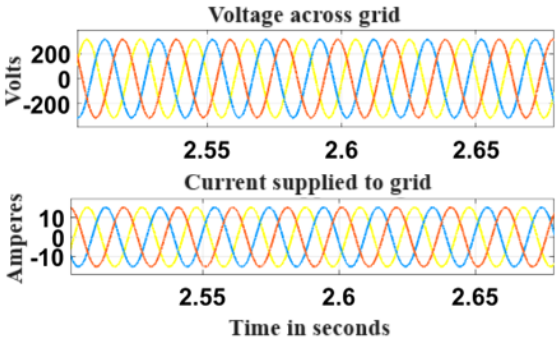

Figure 9. The voltage at PCC and the current injected by DSTATCOM to grid

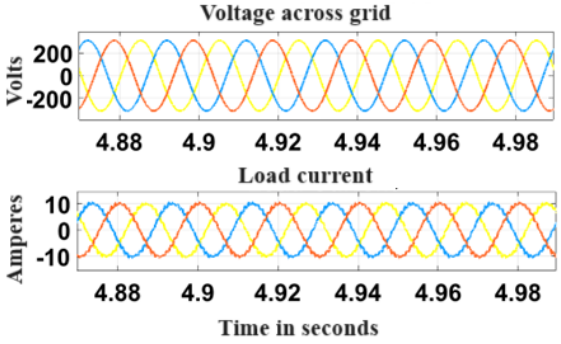

Figure 10. The voltage at PCC and Load Current

Table 3. The Kp and Ki values for the three employed tuning techniques

Method of tuning	Kp	Ki
Ziegler-Nichols Method	0.1	1.3
PSO Algorithm	0.14	1.8
GSA	0.17	1.5

Table 4. Comparison of performance of tuning methods

Method of tuning	Overshoot	Rise Time	Settling time number of oscillation cycles	Steady State Error	ISE
Zeigler Nicholas	72 V	0.43 Seconds	1	28 V	64.30
PSO Algorithm	34 V	0.34 Seconds	2	16 V	32.00
GSA Algorithm	12 V	0.23 Seconds	1	12 V	22.78

A comparison of the performance indices with regard to the regulation of the DC link voltage using the Kp and Ki values obtained by employing the ZN, PSO and GSA techniques is given in Table 4.

Further on, the simulation pertaining to the scaled-down proposed model was also implemented in MATLAB to find out the Kp and Ki values by using the tuning techniques and these values were used for the experimental setup as well.

7. Experimental Validation

The proposed system has been experimentally validated by means of a prototype. The important parameters and specifications forthe experimental prototype are given in Table 5.

The experimental verification model was built based on the PIC16F877A micro controller as the main controller for the DSTATCOM. For the purpose of controlling the SLLC a separate PIC micro controller 16F877A has been used. Figure 11 depicts the scaled-down experimental prototype.

The experimental validation was carried outusing a scaled-down model with a 48 V, 3-phase and50 Hz system derived from the 380 V systems using a three-phase transformer. The DC voltage was maintained at 128 Volts. The DSTATCOM Bridge was implemented using MOSFETs IRF 840. The PI controllers were developed in the Micro controllers and the A0 and A1 and A2 channels of the PIC micro controllers were used for reading the three-phase AC voltage after full wave rectification.

In the experimental setup the solar irradiance was changed from 200 w/m^2 to 800 w/m^2 by

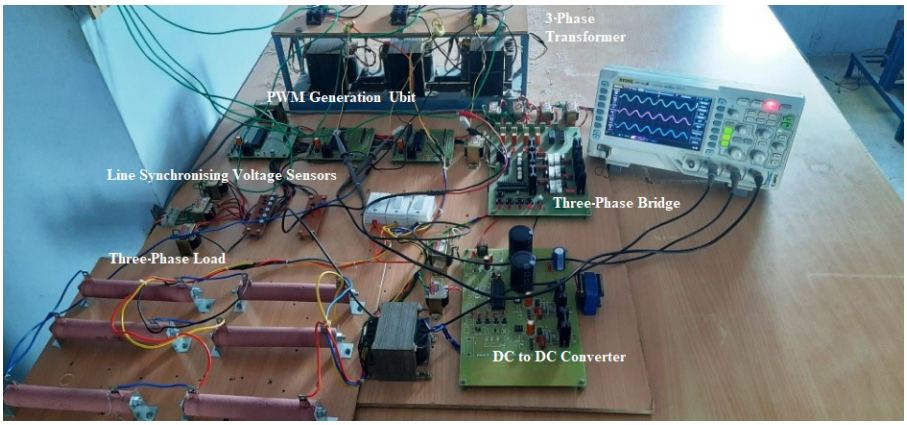

Figure 11. Photograph of the experimental prototype

Table 5. Parameters and specifications for the Experimental Prototype

Parameter	Specification
Renewable energy source	Solar PV Source
Rated maximum Power	250 W
SPV Source Terminal Voltage	21 V
DSTATCOM	
Rated Capacity	1000W
DC Link Voltage	128 V
AC Voltage	48 V; 3 Ph; 50 Hz
RL Filter	L = 10 mH; R = 3 Ohms
Load	250 W; 250 VAR

using an artificial setup and the resulting solar PV current. It can be noticed that the sudden change in the solar irradiance has increased the DC link current thus increasing the power delivered to the DSTTACOM so as to be integrated into the grid. The DC link voltage was regulated at 144 V as shown in Figure 12. On a scale of 1:40 the DC link voltage was regulated at 120 Volts. When the solar irradiance is as low as 200 w/m2 the ripple content of the DC link voltage is enhanced. Figures 13 and 14 show the switching pulses applied to the upper and lower switches of the R-Phase Leg of the converter for the different modulation indices 0.63 and 0.73. It is to be noted that that switching pulses for the two switches on the same leg are complementary in nature. Figure 15 shows the voltages across the nodes of the three-phase converter along with the Fast Fourier Transform (FFT) of the phase voltage. The grid injection current changes once with the change in the intensity of solar irradiance.

8. Conclusion

In this paper a novel methodology for the grid integration of Solar Photo Voltaic Power is presented. The proposed system uses a SLL converter to bring the energy harvested from the SPV source to the DSTATCOM. The conclusions of the carried out simulation are as follows. The sliding mode controller used for MPPT which only requires the measurement of the voltage, has ensured the efficient tracking of the maximum power point. Further on, the tuning of the two PI controllers of the DSTATCOM has been carried out using the GSA. The results of GSA-based tuning were compared with the results of Ziegler-Nichols and of the PSO-based tuning scheme. The results of the simulations and of the experimental verification which were carried out validate the proposed method. By comparing the value of the overshoot, the number of oscillation cycles and the values of the steady state error and Integral Square Error obtained by employing the ZN-, PSO- and GSA-based algorithms, it was established that the GSA-based tuning of the PI controller featured a better performance. A possible future direction of this research could be the implementation of the complete control scheme on a FPGA platform as an embedded system using the PIC Micro controller.

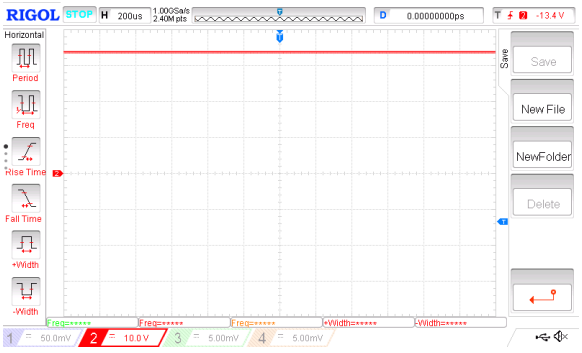

Figure 12. The DC link voltage (1cm = 40 V)

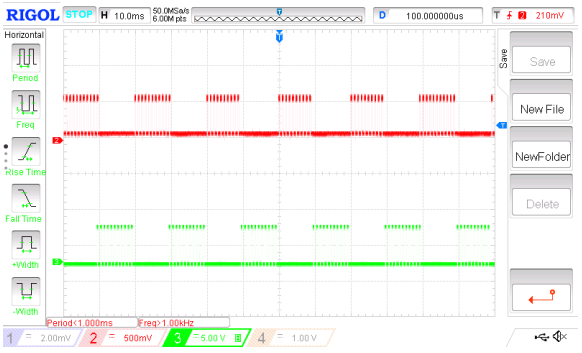

Figure 13. R-PhaseLeg Switch Pulses with MI = 0.63

Figure 14.R-Phase legSwitch pulses with MI = 0.73

Figure 15. DSTATCOM Voltages and FFT

REFERENCES

Amoozegar, D. (2016) DSTATCOM modelling for voltage stability with fuzzy logic PI current controller. *International Journal of Electrical Power & Energy Systems*. 76, 129-135. doi: 10.1016/j.ijepes.2015.09.017.

Badoni, M., Singh, A. & Singh, B. (2016) Adaptive neurofuzzyinference system least-mean-square-based control algorithm for DSTATCOM. *IEEE Transactions on Industrial Informatics*. 12(2), 483-492. doi: 10.1109/TII.2016.2516823.

Baharudin, N. H., Syed Hassan, S. I., Saad, P., Tunku Mansur, T. M. & Ali, R. (2015) A Review on DSTATCOM Neural Network Control Algorithm for Power Quality Improvement. *Applied Mechanics and Materials*. 785, 363-367. doi: 10.4028/www.scientific.net/AMM.785.363.

Bhattacharya, A. & Chakraborty, C. (2011) A shunt active power filter with enhanced performance using ANN-based predictive and adaptive controllers. *IEEE Transactions on Industrial Electronics*. 58(2), 421-428. doi: 10.1109/TIE.2010.2070770.

Coteli, R., Besir, D. & Fikret, A. (2011) Fuzzy-PI current controlled DSTATCOM. *Gazi University Journal of Science*. 24(1), 91-99.

Dheepanchakkravarthy, A., Akhil, S., Venkatraman, K., Selvan, M. P. & Moorthi, S. (2018) Performance Analysis of FPGA Controlled Four-leg DSTATCOM for Multifarious Load Compensation in Electric Distribution System. *Engineering Science and Technology - An International Journal*. 21(4), 692-703. doi: 10.1016/j.jestch.2018.05.004.

Eshtehardiha, S., Bayatipoodeh, M. & Kiyoumarsi, A. (2007) Optimized Performance of STATCOM with PID Controller Based on Genetic Algorithm. In: *International Conference on Control, Automation and Systems, 17-20 October 2007, Seoul, Korea*. IEEE. pp. 1639-1644.

Masand, D., Jain, S. & Agnihotri, G. (2008) Control strategies for distribution static compensator for power quality improvement. *IETE Journal of Research*. 54(6), 421-428. doi: 10.4103/0377-2063.48632.

Myneni, H., Kumar, G. S. & Sreenivasarao, D. (2017) Dynamic DC voltage regulation of split-capacitor DSTATCOM for power quality improvement. *IET Generation, Transmission & Distribution*. 11(17), 4373-4383. doi: 10.1049/iet-gtd.2017.0494.

Naz, M. N., Imtiaz, S., Bhatti, M. K. L., Awan, W. Q., Siddique, M. & Riaz, A. (2021) Dynamic Stability Improvement of Decentralized Wind Farms by Effective Distribution Static Compensator. *Journal of Modern Power Systems and Clean Energy*. 9(3), 516-525. doi: 10.35833/MPCE.2018.00422.

Rashedi, E., Nezamabadi-Pour, H. & Saryazdi, S. (2009) GSA: a gravitational search algorithm. *Information sciences*. 179(13), 2232-2248. doi: 10.1016/j.ins.2009.03.004.

Singh, B. & Arya, S. R. (2014) Back-Propagation Control Algorithm for Power Quality Improvement Using DSTATCOM. *IEEE Transactions on Industrial Electronics*. 61(3), 1204-1212. doi: 10.1109/TIE.2013.2258303.

Singh, B. & Singh, S. (2019) GA-based optimization for integration of DGs, STATCOM and PHEVs in distribution systems. *Energy Reports*. 5, 84-103. doi: 10.1016/j.egyr.2018.09.005.

Srikakolapu, J., Arya, S. R. & Maurya, R (2021) Distribution static compensator using an adaptive observer based control algorithm with salp swarm optimization algorithm. *CPSS Transactions on Power Electronics and Applications*. 6(1), 52-62. doi: 10.24295/CPSSTPEA.2021.00005.

Shen, D. & Lewn, P. W. (2002) Modeling, analysis, and control of a current source inverter-based STATCOM. *IEEE Transactions on Power Delivery*. 17(1), 248-253. doi: 10.1109/61.974214.

Sherin Jasper, S. (2015) Artificial Neural Network Controlled DSTATCOM For Power Quality Improvement. *International Journal of Innovative Research in Electrical, Electronics, Instrumentation and Control Engineering*. 3(5), 150-158. doi: 10.17148/IJIREEICE.2015.3538.

Xu, Y. & Li, F. (2014) Adaptive PI Control of STATCOM for Voltage Regulation. *IEEE Transactions on Power Delivery*. 29(3), 1002-1011. doi: 10.1109/PESGM.2014.6939003.